

Turbulent Bénard-Marangoni Convection: Results of Two-Dimensional Simulations

Thomas Boeck and André Thess

*Center for Physical Fluid Dynamics, Department of Mechanical Engineering, Dresden University of Technology,
01062 Dresden, Germany*

(Received 29 September 1997)

We report long-time direct numerical simulations of two-dimensional Bénard-Marangoni convection at a low Prandtl number driven exclusively by surface tension gradients. At high Marangoni numbers we observe a turbulent flow characterized by a cycle of vorticity generation at the free surface and injection of surface vorticity into the layer. The energy dissipation obeys the Kolmogorov scaling. Our results differ from predictions of a scaling analysis by Pumir and Blumenfeld, but agree with a modified theory which takes the moderate Peclet numbers in the simulations into account. [S0031-9007(98)05322-8]

PACS numbers: 47.27.Eq, 47.20.Dr, 47.27.Cn, 47.27.Te

Rayleigh-Bénard convection has become a paradigm for the study of buoyancy-driven turbulence [1] due to its conceptual simplicity and the unprecedented accuracy with which the scaling law $Nu \propto Ra^{2/7}$ was established both experimentally [2] and theoretically [3–5]. By contrast, very little is known about the turbulent behavior of surface-tension-driven convection in a layer heated from below (Bénard-Marangoni convection) [6,7]. Only a single phenomenological prediction, namely, $Nu \propto Ma^{1/3}$ [8] exists to date, relating the Nusselt number Nu in a turbulent fluid layer with a free upper surface to the Marangoni number Ma . This nondimensional parameter is the analog of the Rayleigh number Ra for surface-tension-driven flows.

In this Letter we report direct numerical simulations which, for the first time, extend sufficiently far into the nonlinear regime to obtain a fully developed turbulent state and to uncover the relevant scaling laws. The prediction of turbulent convection driven by surface tension gradients is of interest in many engineering applications. Examples include welding [9], electron beam melting and evaporation [10], steelmaking [11], and chemical engineering [12]. Moreover, understanding of turbulent Bénard-Marangoni convection may shed new light on other flows driven by surface shear such as wind-driven turbulence [13] and flows in electromagnetically levitated drops [14]. The geometric simplicity of the Bénard-Marangoni problem makes it a prototype system for the study of surface-tension-driven turbulence.

We focus on low-Prandtl-number fluids (liquid metals) typical of most applications mentioned above. Furthermore, we consider two-dimensional motions, an approach that permits us to conduct long-time simulations at very high Marangoni numbers which presently cannot be realized in three dimensions. The utility of two-dimensional simulations for the understanding of turbulent convection has been demonstrated by DeLuca *et al.* [3,4] for the Rayleigh-Bénard problem. Moreover, two dimensionality of the flow can, in principle, be achieved by applying a constant magnetic field parallel to the fluid surface [15].

Our computational model for Bénard-Marangoni convection in a layer $0 \leq z \leq 1$ with periodic boundary conditions in x comprises the following dimensionless equations and boundary conditions:

$$\partial_t \mathbf{v} + (\mathbf{v} \cdot \nabla) \mathbf{v} = -\nabla p + P \nabla^2 \mathbf{v}, \quad (1a)$$

$$\nabla \cdot \mathbf{v} = 0, \quad (1b)$$

$$\partial_t T + (\mathbf{v} \cdot \nabla) T = \nabla^2 T. \quad (1c)$$

$$v_x = v_z = 0, \quad T = 1 \text{ (at } z = 0), \quad (1d)$$

$$v_x = 0, \quad \partial_z T = -1, \quad (1e)$$

$$\partial_z v_x = -Ma \partial_x T \text{ (at } z = 1).$$

Equations (1) are based on the layer thickness d as a unit of length, d^2/κ as a unit of time, and qd/λ as a unit of temperature, where q is the prescribed heat flux at the free surface and λ denotes the heat conductivity of the fluid. Velocity $\mathbf{v} = v_x \mathbf{e}_x + v_z \mathbf{e}_z$ and temperature T depend only on x, z . The Prandtl number $P = \nu/\kappa$ represents the ratio of kinematic viscosity and thermal diffusivity. We assume the relation $\sigma = \sigma_0 - \gamma T$ for the temperature dependence of the surface tension σ . The Marangoni number is defined as $Ma = \gamma q d^2 / \lambda \rho \nu \kappa$, where ρ denotes the density of the fluid. Instability of the basic state $\mathbf{v} = 0, T = 1 - z$ occurs above $Ma_c \approx 79.6$ for a wave number $k_c \approx 1.99$ [6]. Since the heat flux is prescribed, convection reduces the temperature difference across the layer. Therefore, the Nusselt number is defined as

$$Nu = 1/\langle \Delta T \rangle. \quad (2)$$

where $\langle \Delta T \rangle$ denotes the mean temperature difference between the bottom and free surface. Both system (1) and the system investigated in [16] are translationally invariant with respect to x . The important difference between them consists of the boundary condition $v_x = 0$ at the bottom of the layer. When it is replaced with $\partial v_x / \partial z = 0$ (free slip), only steady flows are obtained. In contrast to the free-slip case, linear momentum is not a

conserved quantity, i.e., the mean flow

$$Q = \int_0^1 v_x dz \quad (3)$$

can become nonzero. Translational invariance is usually broken in practical situations, e.g., by lateral walls. Nevertheless, the results should have some relevance for situations where the effect of the walls is weak, e.g., in large aspect ratio containers.

We solve the system (1) numerically by using a pseudospectral Fourier-Chebyshev method. In order to ensure high resolution with a moderate number of modes, we have selected the small periodicity length $L = 2$. The corresponding critical Marangoni number is $Ma \approx 101.3$. We choose $P = 0.1$ as a compromise between the more realistic value $P = 0.01$ with only a modest achievable Peclet number Pe and the unrealistic value $P = 1$, which permits one, however, to obtain $Pe \gg 1$. We have explored the parameter space up to $Ma = 1.2 \times 10^5$, which corresponds to three decades above the onset of instability. At present, this cannot be achieved in three-dimensional simulations. In terms of advective time scales, the simulations have been run significantly longer than previous Rayleigh-Bénard simulations [3–5]. Table I shows that the present numerical results cover several hundred large-scale eddy turnover times.

Our simulations suggest a rough division into two parameter ranges with significantly different behavior of the system. This is reminiscent of “soft” and “hard” turbulence in Rayleigh-Bénard convection [3,4]. For $Ma < 4 \times 10^4$ we find the scaling exponent for Nu on Ma to be close to the inertial value $1/3$ [16]. This inertial or flywheel regime is replaced by a turbulent regime beyond $Ma \approx 4 \times 10^4$.

Let us briefly describe the inertial case before analyzing the turbulent case. For slightly supercritical values of the Marangoni number, the flow pattern takes the form of steady rolls. Upon increasing Ma , the dynamics becomes increasingly complex. We first observe laterally traveling rolls with $Q \neq 0$. Later, the motion becomes oscillatory. Regardless of the temporal dynamics, the inertial flow pattern is characterized by flat vorticity distributions in the interior of the rolls. Energy input and dissipation in one

TABLE I. Data from turbulent runs. Numerical resolution is 512×129 collocation points. Total time t_{run} in units d^2/κ ; n denotes the number of roll turns estimated from the time $4d/\bar{v}$ for a single turn with rms velocity. ε , Re , and Nu represent averages over t_{run} . ε is measured in units κ^3/d^4 .

Ma	t_{run}	n	Re	Nu	ε
4.0×10^4	13.8	236	684	5.24	5.62×10^4
5.0×10^4	12.9	231	717	5.30	7.58×10^4
6.0×10^4	17.6	344	781	5.41	9.75×10^4
8.0×10^4	15.9	359	903	5.79	1.42×10^5
1.0×10^5	12.7	312	983	5.63	2.01×10^5
1.2×10^5	11.8	316	1073	5.84	2.59×10^5

turnover of the rolls are small compared with the total kinetic energy of the flow. The surface shear accelerates the fluid along the surface towards the maxima of surface tension corresponding to the minima of surface temperature. In this way, sheets of opposite vorticity are generated at the free surface, which supply energy to rolls beneath them. These vortex sheets meet in stagnation points and inject jets of fluid into the bulk. Interaction between the lateral motion of the rolls and the jets is responsible for the rich dynamic behavior of the system. Figure 1 contains an example of quasiperiodic dynamics governed by two processes on different time scales, namely, a short-time oscillation of the size of the rolls seen in the Nusselt number plot in Fig. 1(a) and a long-time oscillation of the amplitude of the mean flow shown in Fig. 1(b). Because of the inertial character of the flow, many roll turnovers are required for a relatively large change in the energy associated with the long-time oscillation.

In the turbulent regime we observe complex spatial and temporal dynamics. Figures 1(a) and 1(b) demonstrate the irregular temporal evolution of Nu and Q , in contrast to the quasiperiodic regime. In spite of the spatiotemporal irregularity, reversals of the mean flow on very long (viscous) time scales persist in the flow. This behavior resembles the random rotational motion of the mean flow

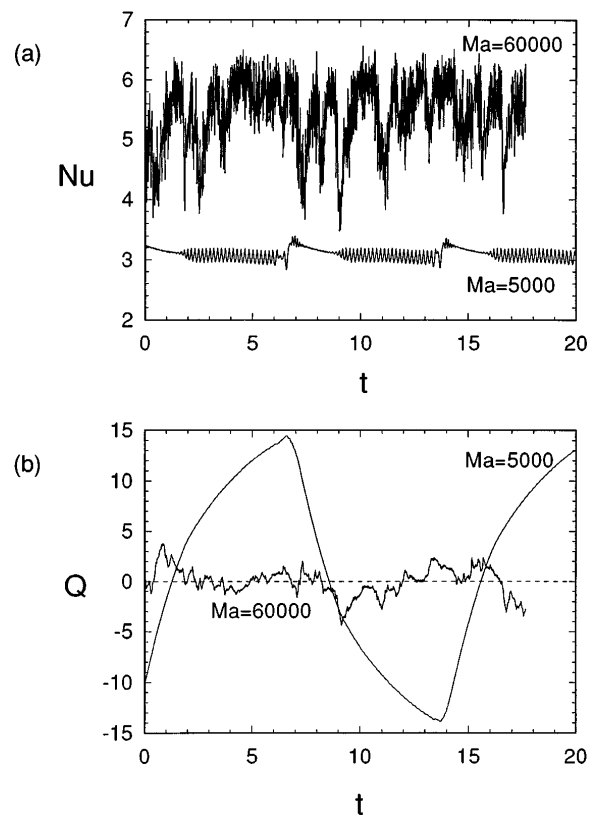


FIG. 1. Temporal evolution of Nu and the mean flow Q in the quasiperiodic ($Ma = 5 \times 10^3$) and turbulent case ($Ma = 6 \times 10^4$). Notice the slow dynamics in Q . [(a) and (b), see text.]

in Rayleigh-Bénard convection at a low Prandtl number [17]. Spatial irregularity and scale separation as characteristic features of turbulent motion are obvious from the snapshots of the vorticity field $\omega = \partial_x v_z - \partial_z v_x$ shown in Fig. 2. They also demonstrate the mechanism of the turbulent dynamics. In the upflow stagnation region at the free surface, new vorticity is generated because of the thermocapillary instability. The slow lateral motion of the rolls drags fluid from this region into a vortex sheet, which amplifies the perturbation and advects it towards the downflow region. In this way, blobs of vorticity form at the free surface, which are injected into the layer [cf. the central white blob of vorticity at the free surface in the upflow region in Fig. 2(a) and its position in Fig. 2(b)]. Distorting bulk motion disrupts the jet as it penetrates the layer [Fig. 2(c)]. As a result, vortices are generated, which are swept across the bulk by the large-scale circulation.

Transition to turbulent behavior is reflected in the integral quantities shown in Fig. 3. Here, the average energy dissipation rate per unit mass ε is plotted as a function of the Reynolds number Re , and Re and Nu are shown as functions of Ma . All three quantities are temporal averages from the runs listed in Table I. The Reynolds num-

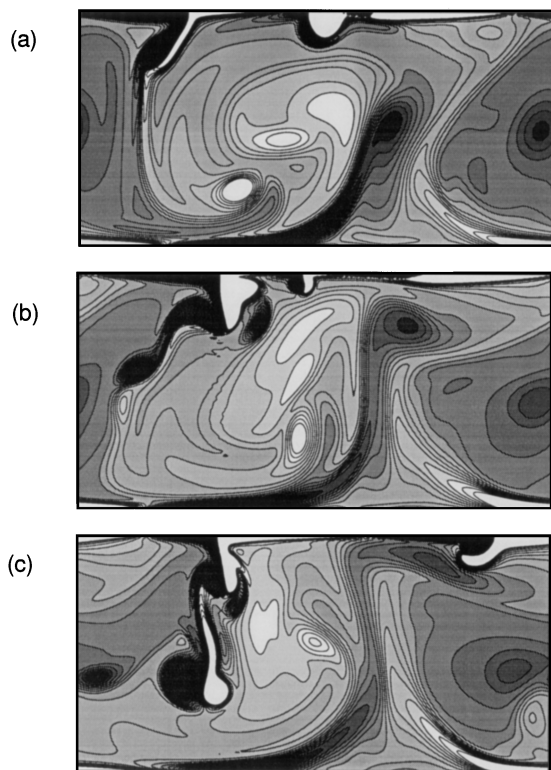


FIG. 2. Vorticity snapshots for $Ma = 6 \times 10^4$. Black and white corresponds to large negative and positive values. The downward jet corresponds to the black and white “strips” branching off the upper surface. Injection of surface vorticity into the layer is exemplified by the motion of the central white blob of vorticity at the free surface in (a). [See text for an explanation of (a)–(c)].

ber $Re = \bar{v}/P$ is based on the rms (integral) velocity \bar{v} defined by

$$\bar{v}^2 = \frac{1}{t_{\text{run}} L} \int_0^{t_{\text{run}}} \int_0^1 \int_0^L v^2(x, z, t) dx dz dt. \quad (4)$$

In our dimensionless units, the quantity ε is given by $\varepsilon = P \bar{\omega}^2$ with the same definition of the overbar symbol as in Eq. (4). Data from the inertial regime ($Ma = 10^4$ up to $Ma = 3 \times 10^4$) are fitted by the relations

$$\varepsilon \propto Re^{2.2}, \quad Re \propto Ma^{0.58}, \quad Nu \propto Ma^{0.30}, \quad (5)$$

whereas for the turbulent regime ($Ma \geq 4 \times 10^4$) we obtain

$$\varepsilon \propto Re^{3.2}, \quad Re \propto Ma^{0.43}, \quad Nu \propto Ma^{0.10}. \quad (6)$$

The turbulent character of the flow changes the ε scaling on Re . The observed relation $\varepsilon \propto Re^{3.2}$ is close to the relation $\varepsilon \propto Re^3$ from Kolmogorov’s phenomenological theory, indicating a state of developed turbulence. Notice that the specific form $\varepsilon \propto Re^3$ arises upon nondimensionalization from $\varepsilon \propto U^3/d$ in dimensional units [18], where U denotes the integral velocity. The more efficient energy dissipation in the turbulent regime affects the scaling of

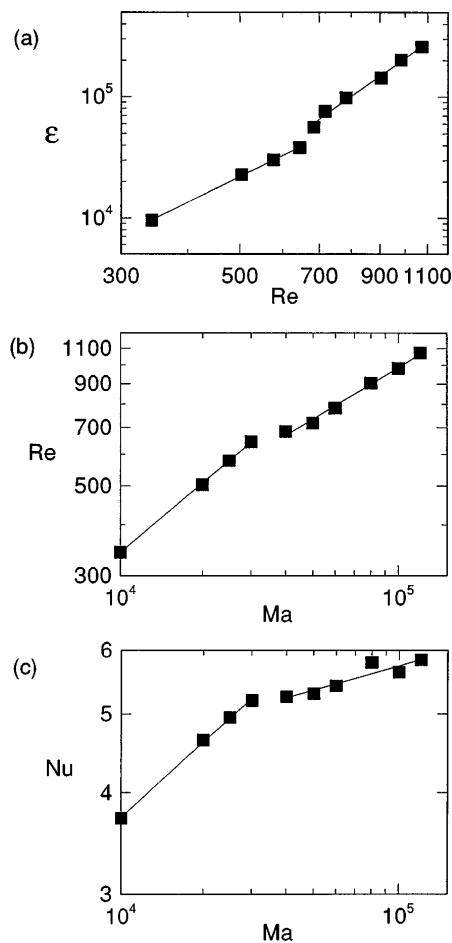


FIG. 3. Power law scaling of the energy dissipation rate ε per unit mass vs the Reynolds number Re (a), and Re (b) and Nu (c) vs Ma .

the other quantities on Ma. In the turbulent regime the growth of Re and Nu with Ma is slowed down. The predictions,

$$\text{Re} \propto P^{-2/3} \text{Ma}^{1/3}, \quad \text{Nu} \propto P^{1/3} \text{Ma}^{1/3}, \quad (7)$$

of Pumir and Blumenfeld [8] are not verified by our result (6). They assume turbulent transport of both momentum and heat, i.e., they consider the limit of large Re and Pe. The Kolmogorov scaling of energy dissipation in our simulations indicates turbulent momentum transport. However, since Pe is smaller by a factor of P compared with Re, the transport of heat may not yet be turbulent. In fact, a modification of the phenomenological model of [8] substituting heat transport through laminar thermal boundary layers for turbulent heat transport gives better agreement with our data, as we now show.

As a first step in the derivation, we observe that production and dissipation of kinetic energy balance in a statistically stationary state. This implies

$$-\text{Ma} \int_0^L v_x \partial_x T dx = P^{-1} \int_0^1 \int_0^L \varepsilon dx dz, \quad (8)$$

where the surface integral on the left-hand side corresponds to the production of kinetic energy due to the Marangoni effect, and the right-hand side represents turbulent viscous dissipation. We assume that $\varepsilon = Cu^3$, where C is a dimensionless constant, and that the surface velocity is of the same order as the average velocity u in the bulk. The free surface dynamics suggests a strong correlation between surface velocity and surface temperature gradients. Therefore we take $\text{Ma}u\langle\partial_x T\rangle L$ as an estimate of the production term, where $\langle\partial_x T\rangle$ denotes the rms average of the horizontal temperature gradient at the free surface. The temperature field is assumed constant in the bulk with thermal boundary layers at the top and bottom surfaces. The thickness of the top layer is of order $1/\sqrt{u}$. Since $\partial_z T = -1$ at the top surface, the total temperature difference between top and bottom is of order $1/\sqrt{u}$, hence $\text{Nu} \propto \sqrt{u}$. Moreover, $L\langle\partial_x T\rangle$ is assumed to be of the same order as the temperature drop across the boundary layer. Our estimate for the energy production term is therefore $\text{Ma}\sqrt{u}$. Using Eq. (8) and $\text{Re} \propto u/P$, we obtain the modified scaling relations

$$\text{Re} \propto P^{-3/5} \text{Md}^{2/5}, \quad \text{Nu} \propto P^{1/5} \text{Ma}^{1/5}. \quad (9)$$

Our numerical results (6) for the scaling of Re with Ma are in reasonable agreement with (9), but the exponent for Nu is significantly less than $1/5$. This discrepancy is probably related to slow convergence for the average values of Nu because of the large fluctuations in Nu shown in Fig. 1(a). Notice that the predicted exponents of P in (9) are based on the universality of C [18]. Nonuniversality will modify the P dependence in (9).

As a final observation we mention that, from the description of the system using Kolmogorov scaling, one may infer that a finite energy dissipation rate is maintained in the small viscosity limit. This property is remarkable from the viewpoint of two-dimensional

turbulence, since the two-dimensional Euler equation is regular, implying that the energy cascade to low wave numbers is normally incompatible with a statistically stationary state [19]. We attribute the finite energy dissipation rate in two-dimensional Bénard-Marangoni convection to the generation of (singular) vortex sheets in the inviscid limit. This becomes apparent when the Marangoni boundary condition is written in the dimensional form $\omega = \gamma \partial_x T / \nu$.

In summary, we have reported direct numerical simulations of turbulent Bénard-Marangoni convection. We find Kolmogorov scaling for the energy dissipation for Marangoni numbers between 4×10^4 and 1.2×10^5 . The scaling laws for Reynolds and Nusselt numbers differ from the prediction of [8] since heat transport through laminar boundary layers has not yet been replaced by turbulent heat transport.

We are grateful to Ch. Karcher, N. Kukharkin, and A. Pumir for interesting discussions. Financial support from the Deutsche Forschungsgemeinschaft under Grants No. Th 497/9-1 and No. Th 497/9-2 is acknowledged.

-
- [1] E. D. Siggia, *Annu. Rev. Fluid Mech.* **26**, 137–168 (1994).
 - [2] B. Castaing, G. Gunaratne, F. Heslot, L. Kadanoff, A. Libchaber, S. Thomae, X.Z. Wu, S. Zaleski, and G. Zanetti, *J. Fluid Mech.* **204**, 1–30 (1989).
 - [3] E. E. DeLuca, J. Werne, R. Rosner, and F. Cattaneo, *Phys. Rev. Lett.* **64**, 2370–2373 (1990).
 - [4] J. Werne, E. E. DeLuca, R. Rosner, and F. Cattaneo, *Phys. Rev. Lett.* **67**, 3519–3522 (1991).
 - [5] R. M. Kerr, *J. Fluid Mech.* **310**, 139–180 (1996).
 - [6] J. R. A. Pearson, *J. Fluid Mech.* **4**, 489–500 (1958).
 - [7] S. H. Davis, *Annu. Rev. Fluid Mech.* **19**, 403–435 (1987).
 - [8] A. Pumir and L. Blumenfeld, *Phys. Rev. E* **54**, R4528–R4531 (1996).
 - [9] T. DebRoy and S. A. David, *Mod. Phys.* **67**, 85–112 (1995).
 - [10] S. Schiller, U. Heisig, and S. Panzer, *Electron Beam Technology*, (Wiley, New York, 1982).
 - [11] J. Szekely, *Fluid Flow Phenomena in Metals Processing*, (Academic, New York, 1979).
 - [12] D. A. Edwards, H. Brenner, and D. T. Wasan, *Interfacial Transport Processes and Rheology*, (Butterworth-Heinemann, Boston, 1991).
 - [13] V. Borue, S. A. Orszag, and I. Staroselsky, *J. Fluid Mech.* **286**, 1–23 (1995).
 - [14] A. D. Sneyd and H. K. Moffatt, *J. Fluid Mech.* **117**, 45 (1982).
 - [15] F. H. Busse and R. M. Clever, *J. Fluid Mech.* **102**, 75–83 (1981).
 - [16] T. Boeck and A. Thess, *J. Fluid Mech.* **350**, 149 (1997).
 - [17] S. Cioni, S. Ciliberto, and J. Sommeria, *J. Fluid Mech.* **335**, 111–140 (1997).
 - [18] U. Frisch, *Turbulence*, (Cambridge University Press, Cambridge, England, 1995).
 - [19] C. R. Doering and J. D. Gibbon, *Applied Analysis of the Navier-Stokes Equations*, (Cambridge University Press, Cambridge, England, 1995).